Solar Energy Materials & Solar Cells 235 (2022) 111457

Contents lists available at ScienceDirect

Solar Energy Materials and Solar Cells

journal homepage: www.elsevier.com/locate/solmat

Tunable thermal management based on solar heating and radiative cooling

Bin Zhao [a], Mingke Hu [b], Qingdong Xuan [c], Trevor Hocksun Kwan [a], Yousef N. Dabwan [a], Gang Pei [a,*]

[a] Department of Thermal Science and Energy Engineering, University of Science and Technology of China, Hefei, 230027, China
[b] Department of Architecture and Built Environment, University of Nottingham, University Park, Nottingham, NG7 2RD, UK
[c] School of Automotive and Transportation Engineering, Hefei University of Technology, 193 Tunxi Road, Hefei, 230009, China

ARTICLE INFO

Keywords:
Solar heating
Radiative cooling
Tunable thermal management
Spectral selectivity

ABSTRACT

Solar heating (SH) and radiative cooling (RC) have been regarded as promising clean techniques for thermal energy harvesting and temperature control. However, SH and RC are only a single function of heat collection and dissipation, which means the static device of SH and RC cannot meet the dynamic heat requirement of real-world applications, especially in the daytime. Here, a strategy of dynamic integration of SH and RC is proposed for tunable thermal management. A device (i.e., SH/RC device) that includes a silica cavity, ultrapure single-walled carbon nanotubes (SWCNTs) aqueous dispersion, solar reflective film, and deionized water is designed and fabricated. The outdoor experimental results show that the SH/RC device with SWCNTs media can effectively achieve heat collection with a maximum temperature of 78.9°C, while the SH/RC device with deionized water can achieve heat dissipation. Besides, the temperature modulation ability of the SH/RC device is tested to be 26.3°C and can be theoretically improved to be 60.3°C by improving the solar absorptivity (i.e., 0.9 for SH mode and 0.1 for RC mode) regulation ability of the device and improving its thermal emissivity (i.e., 0.9). Furthermore, annual analysis indicates that the cumulative time in which the SH/RC device temperature is in a comfortable region (i.e., 20°C-26°C) for humans is 60.9% and 30.3% higher than that of the device with individual SH and RC mode. In summary, this work provides alternative thinking for tunable thermal management based on the dynamic utilization of the hot sun and cold universe.

1. Introduction

Thermal energy exists in various backgrounds of society and is one of the indispensable types of energy for humans. For example, buildings require space cooling and heating all the time and these thermal energy requirements account for nearly 50% of total building energy consumption and are also responsible for the increasing greenhouse gas emission [1]. Thus, exploring the methods to obtain thermal energy that includes heating and cooling based on clean techniques is vital for the sustainable development of society. Generating heat from the sun by the solar heating (SH) method is one of the promising ways for heat generation [2–6]. Recently, exploring the cold universe, the ultimate heat sink, by radiative cooling (RC) for the hardness of the cold has also attracted much attention since the cooling phenomenon can be obtained passively by RC without additional energy input [7–11].

Reviewing the previous work, SH has been widely used in the field of solar energy harvesting. The basic principle of the SH is that solar irradiance is absorbed by the solar absorptive materials and then be transferred into heat for the end-user. The key to achieve SH is that the material needs to have high solar absorptivity, and there are a variety of solar absorptive materials for the SH technique, including black paint [12], multilayer selective solar absorber [13,14], and nano/micro fluids [15,16]. On the energy system level, the SH method has been integrated into different systems and applications, such as flat-plate solar collectors for water hot and space heating [17], parabolic trough solar collectors for power generation [18], porous/coating-based black devices for desalination of seawater [19]. In the field of energy-saving buildings, SH has been applied to collect clean hot water and provide space heating so that the building energy consumption can be significantly reduced. Recently, RC has been developed to explore the coldness of the universe for passive cooling, and large amount studies have been devoted to the development of RC. The main principle of the RC is that radiative coolers can dissipate heat into the universe directly based on the transparency of the atmospheric window, thus, a cooling phenomenon is passively

* Corresponding author.
E-mail address: peigang@ustc.edu.cn (G. Pei).

https://doi.org/10.1016/j.solmat.2021.111457
Received 6 September 2021; Received in revised form 8 October 2021; Accepted 18 October 2021
Available online 26 October 2021

obtained. According to the thermal analysis, strictly spectral tailoring of the radiative cooler is the key for effective RC, and high-performance radiative coolers that include multilayer films [20,21], photonic coolers [22,23], metamaterials [24], and porous polymers [25,26] have been successfully developed. Besides, RC has been used in various applications, such as photovoltaic cooling [27,28], personal thermal management [29], water collection [30], and building energy-saving [31]. For example, experimental demonstrates show that a building-integrated RC system can save electricity by over 15% [32], and a radiative cooled-cold collection system with kW-scale cooling power is developed for building energy-saving [33].

Although SH and RC are clean ways for effective heat collection and heat dissipation, respectively, the thermal management characteristic of them are static, which means SH can only be used for heat collection, while RC can only be used for heat dissipation. In real-world applications, thermal energy requirements are dynamically changed due to various factors, such as season variations. For example, buildings located in the "hot summer and cold winter" regions need heat collection mode in the cold winter, while heat dissipation mode is preferred in the hot summer. Thus, SH and RC are not suitable for the demand of dynamic thermal management, so developing smart and renewable ways for tunable thermal management is urgently needed. To achieve this goal, combining SH and RC modes into a single device with a switchable way is an interesting topic and many researchers have made contributions [1,34–39]. Zhou et al. [34] proposed an RC and SH coupling module to directly control the indoor temperature of buildings. The proposed module has two surfaces that exhibit different spectral properties, one surface is solar absorbing material, the other is a radiative cooler. Simulation results showed that electricity consumption can be saved by 42.4% in the cooling season with the module, and that can be improved to be 63.7% when coupling with an energy storage system. Hsu et al. [1] developed a dual-mode device with electrostatically-controlled thermal contact conductance. A solar absorber and radiative cooler are attached on the same substrate side by side, and the roller driven by the electrically controlled motor is used to select different surfaces for application, corresponding to the switchable of the SH and RC mode. The above works mainly use a mechanically rotated structure to switch the SH mode and RC mode based on the individual solar absorber and radiative cooler. On the level of the material, Wang et al. [37] proposed a self-adaptive compound metasurface for the dynamic combination of SH and RC. The metasurface consists of a large cross resonator and a small cross resonator. The large cross resonator is responsible for the absorption adjustment, while the small cross resonator is responsible for the thermal emission. The metasurface behaviors like a radiative cooler when the surface is at a high level, while it acts as a solar absorber when the surface is at a low level, achieving a self-adaptive thermal control. This work is a conceptual development, experimental demonstrations are required for validation. Long et al. [38] proposed a smart window with a switchable front side LWIR emissivity and solar modulation ability based on a sandwich structure that mainly consists of ITO and hydroxypropyl cellulose hydrogel part for tunable thermal management and daylighting when coupled with mechanical flip strategy. This kind of hydrogel-based material can be also used for thermal homeostasis applications [39]. Based on the above analysis, it can be found that the research on the dynamic combination of SH and RC is still at an early stage, and more contributions should be further made. Besides, most of the above-reported works involve complicated materials (e.g., photonic materials) and structures (e.g., shutter structure), which means the ultraprecision fabrication process and rotatable components are highly required.

In this paper, a tunable thermal management strategy is proposed by integrating the volume absorption of media and general radiative cooler for the dynamic combination of SH and RC, which is easy to operate without any complicated materials and structures. Then, a device that combines SH and RC (referred to as "SH/RC device" hereinafter) based on the transparent silica cavity, ultrapure single-walled carbon nanotubes aqueous dispersion, and deionized water is designed and fabricated. Outdoor testings are conducted to compare the operation temperature of the SH/RC device under SH and RC modes. Besides, a validated model is also used to predict the temperature of the device under different parameters, as well as the tunable temperature management ability evaluation. Moreover, an annual simulation is performed to show the tunable temperature management performance of the proposed strategy.

2. Experimental section

2.1. Description of the tunable thermal management strategy

The tunable thermal management process is designed to be achieved by the switchable utilization of SH and RC, and the schematic of the strategy is shown in Fig. 1. It can be seen that the tunable thermal management strategy is obtained based on an integrated SH/RC device that includes transparent cooler, encapsulating material, solar reflector, and media. The transparent cooler needs to have high solar transmittance and thermal emissivity, the encapsulating material should have high solar transmittance, while the solar reflector needs to have a strong solar reflection. Besides, the media needs to have high solar absorption in SH mode, while the media should be optically transparent in RC mode. The detailed tunable thermal management strategy is described as follows:

(i). In SH mode, the SH/RC device is filled with media that has strong solar absorption so that the transmitted sunlight can be directly absorbed. Besides, the solar reflector can also improve the solar absorption of the media since it can enlarge the optical length of the sunlight in the media. Therefore, the device and its media are heated up by absorbed solar power.

(ii). In the RC mode, the SH/RC device is filled with transparent media that has no solar absorption so that the incident sunlight can transmit the transparent cooler and media and then be highly reflected by the solar reflector. Meanwhile, the transparent cooler can emit strongly within the mid-infrared wavelength band. Thus, the device and its media can be radiatively cooled.

(iii). During the tunable thermal management process, different types of media can switchably be used according to the heat and temperature demand of applications. Importantly, this kind of strategy can be integrated into a loop-locked structure or system for tunable thermal management or temperature control.

2.2. Materials and spectral characterization

In this work, 1-mm-thick bulk silica is selected as the transparent cooler since silica is optically transparent and has high thermal emissivity. Besides, the 1-mm-thick bulk silica is also chosen as the encapsulating material. A metamaterial film [24] that has high solar reflection is selected as the solar reflector. As for the media, carbon nanotubes (CNTs)-based fluid is selected for SH mode, and deionized water is selected for RC mode. CNTs -based fluid is the ultrapure single-walled carbon nanotubes (SWCNTs) aqueous dispersion (XFNANOR) with a mass fraction of 0.15%. The outside diameter of the CNT is 1–2 nm and the length of the CNT is approximately 5–30 μm.

To investigate the radiative properties of the selected materials, the spectral reflectivity and transmittance of the selected materials are measured, and the spectral absorptivity and emissivity are obtained using the energy balance law and Kirchhoff`s law. In the solar radiation band (i.e, 0.3–2.5 μm), the reflectivity and transmittance of the bulk silica and metamaterial film are measured using the UV–Vis–NIR spectrophotometer (SolidSpec-3700, Shimadzu) with a spectral resolution of 1 nm. In the mid-infrared wavelength band, the reflectivity and transmittance of the bulk silica and metamaterial film are tested using a Fourier Transform Infrared Spectrometer (Nicolet iS50, Thermo

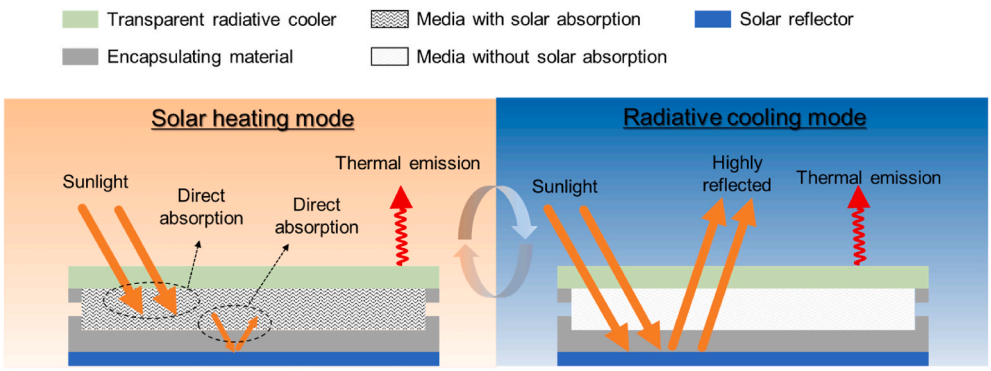

Fig. 1. The schematic of the SH/RC device and tunable thermal management strategy.

Scientific) coupled with an integrating sphere (Mid-IR IntegratIR, Pike Technologies). As shown in Fig. 2a, the bulk silica possesses a high solar transmittance with an averaged transmittance of about 93.8%, corresponding to low solar reflectivity. Fig. 2b shows that the bulk silica has a strong thermal emission in the mid-infrared wavelength band except for wavelength near 9 μm where an emissivity drop occurs. To validate the above-measured data, an optical simulation based on the transfer matrix method is conducted and the simulated results are in good agreement with the test data. The optical constants of the silica used for simulation are extracted from the optical handbook [40].

The solar transmittance of the CNTs-based fluid and deionized water are shown in Fig. 3. During the measurement, the 10-mm-thick cuvette is used for liquid testing. It is observed that the deionized water has a high optical transmittance, while the CNTs-based fluid is opaque for the light under testing conditions, which reveals that the CNTs-based fluid can be potentially used for light trapping and then solar thermal conversion. Notably, the transmittance of the deionized water decrease when the wavelength increases to the near-infrared band and this indicates that there exists an intrinsic absorption of the water within the near-infrared wavelength band, and this will increase the temperature of the SH/RC device under RC mode. So, compared with deionized water, media with lower solar absorptivity is more preferable for the SH/RC device under RC mode.

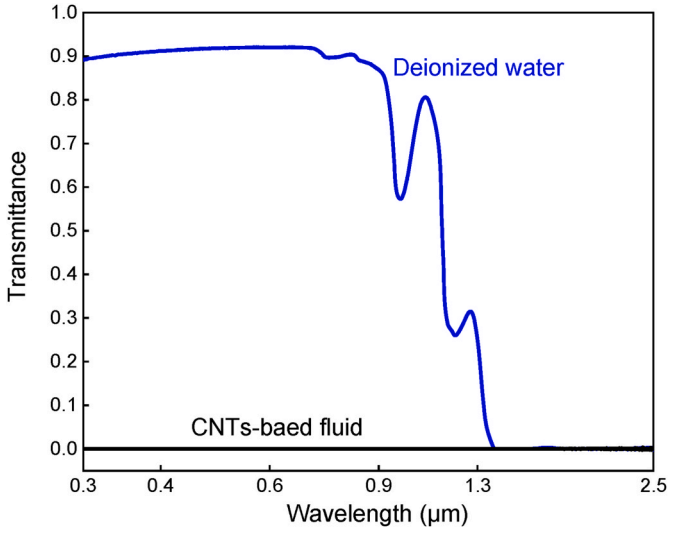

Fig. 3. Measured solar transmittance of the CNTs-based fluid and deionized water. During the measurement, the 10-mm-thick cuvette is used for the sample holder.

2.3. Experimental setup

The photo and schematic of the experimental setup are shown in Fig. 4. The SH/RC device is placed into the aperture of the thermal insulation material (i.e., polystyrene foam) and a polyethylene (PE) film is fixed on the top surface. The highly transparent PE film acts as a windshield that can significantly reduce the convection heat transfer process between the SH/RC device and local air so that the effect of radiation heat transfer mode on the tunable thermal management can be highlighted. The out surface of the setup is covered by aluminum foil to reduce unnecessary solar absorption.

As shown in Fig. 4, if the SH/RC device is filled with CNTs-based fluid, it looks like a black surface and can be used to absorb sunlight

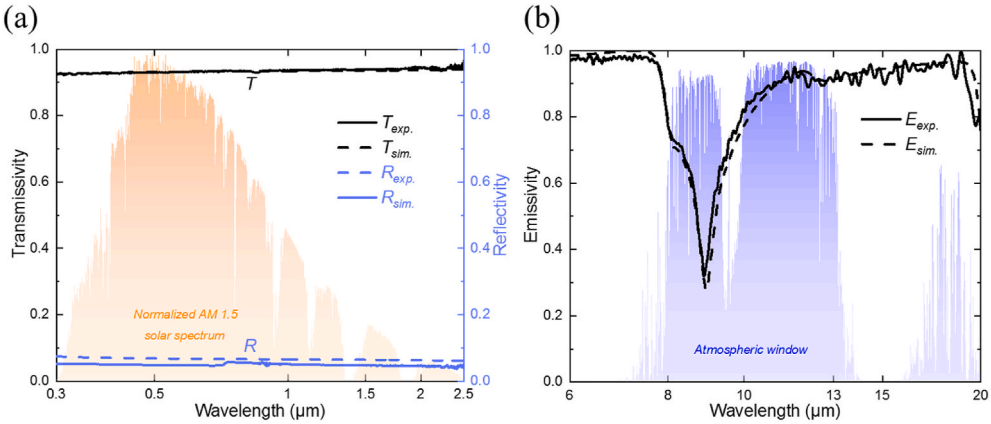

Fig. 2. The spectral properties of the 1-mm-thick silica. (a) Measured solar reflectivity and transmittance, and (b) measured thermal emissivity of the 1-mm-thick silica with simulated results plotted as reference.

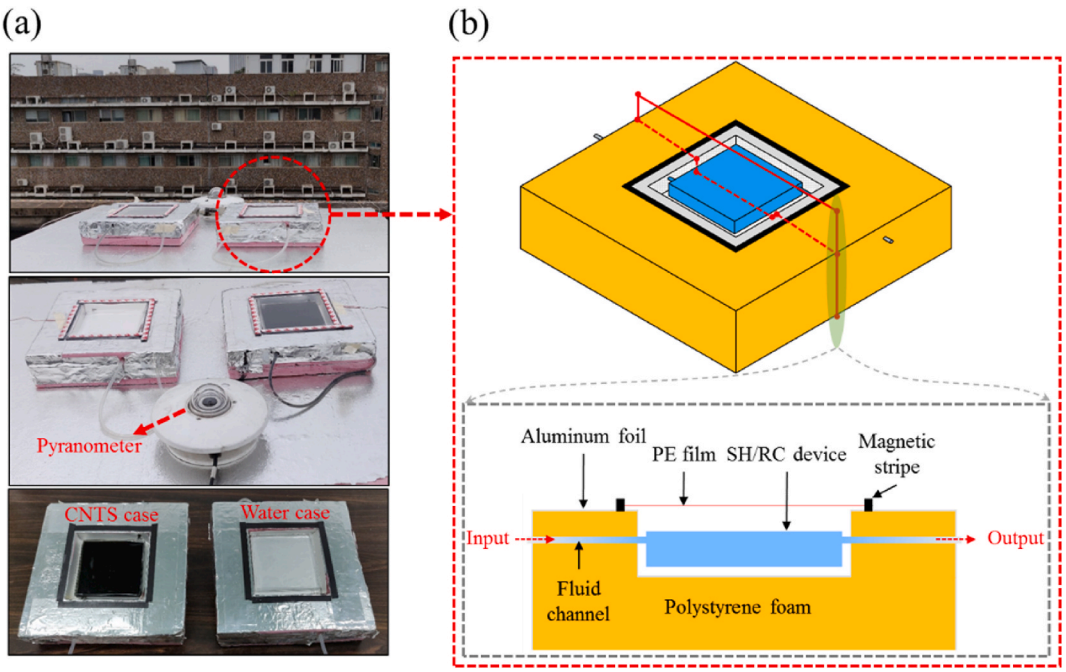

Fig. 4. Photo and schematic of the experimental setup.

to improve the temperature, we call it "*CNTs case*". However, if the SH/RC device is filled with deionized water, it looks like a highly transparent surface so that the sunlight can be highly reflected by the metamaterial film fixed on the bottom surface, thus the temperature of the device can be maintained at a relatively low level, we call it "*Water case*".

The experimental setup is set on the rooftop of the second building of Mechanics in the University of Science and Technology of China at Hefei, China. The temperature of the SH/RC device is monitored by T-type thermocouples that are attached to the backside of the device. The accuracy of the temperature measuring is ±0.5°C. The solar irradiance is measured using the pyranometer (TBQ-2, Jinzhou Sunshine Technology Co.Ltd) and the wind speed is measured using the wind speed sensor (HSTL-FS01). The accuracy for the pyranometer is ±2%. The ambient temperature and relative humidity are measured using an integrated weather station (HSTL-BYXWS). The accuracies for ambient temperature and relative humidity are ±4.5% and ±0.5°C, respectively. The measured data are recorded by a data logger (LR8450, HIOKI) with a time step of 10 s.

2.4. Experimental results

One-day testing was conducted from 02:00 May 8th, 2021 to 19:00 May 8th, 2021. The measured solar irradiance (defined as G in Fig. 5a), relatively humidity (defined as RH in Fig. 5a), and wind speed (defined as u_a in Fig. 5a) are plotted in Fig. 5a. It is found that the solar irradiance seems near perfect within the testing period except for several special points. It is noted that the vibration of solar irradiance at the beginning of the morning is near-linearly and this is because there exists a shadow that is caused by the adjacent building and covers the monitor window of the pyranometer so that the direct solar irradiance is blocked. Besides, the wind speed at daytime is relatively large with an average value of 0.9 m s^{-1}. Moreover, the relative humidity changes with the region of 34.9%–68.4%.

The measured temperature of the SH/RC device under the *CNTs case* and the *Water case* is presented in Fig. 5b with measured ambient temperature plotted as reference. The ambient temperature changes slowly during the testing period. The maximal temperature, minimum temperature, and average temperature of ambient air are 34.4°C, 20.0°C, and 26.6°C. It is clear that the temperature of the SH/RC device under the *CNTs case* is obviously higher than that under the *Water case* at

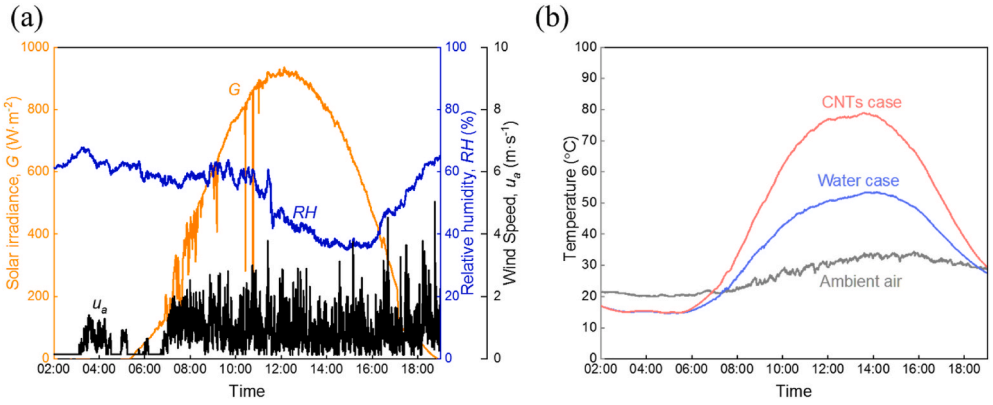

Fig. 5. (a) Measured solar irradiance, relative humidity, and wind speed. (b) Measured temperature of SH/RC device under the *CNTs case* and the *Water case*, with ambient air temperature plotted as reference.

daytime, indicating that the proposed strategy can do regulate the temperature of the SH/RC device. For instance, the maximum temperature of the SH/RC device under the *CNTs case* is 78.9°C, which is 25.5°C higher than that under the *Water case*. Besides, the maximum temperature difference of the SH/RC device between the *CNTs case* and the *Water case* is 26.3°C, showing that the proposed strategy has a strong temperature regulation ability. Besides, the temperature of the SH/RC device under the *CNTs case* and the *Water case* are nearly consistent at night and the temperature difference between the SH/RC device and ambient air is 5.3°C, which is caused by the RC process. Notably, it is found that the temperature of the SH/RC device under the *Water case* is higher than ambient temperature, which indicates that the current SH/RC device under the *Water case* can't achieve a sub-ambient cooling phenomenon. There are three possible reasons for this result. The first reason is that the fabricated silica SH/RC device has a nonnegligible solar absorption since there are uncleanable defects (e.g., dirt) on the inside surface of the device during the high-temperature silica melting process and the water still has a non-negligible volume absorption within the near-infrared wavelength region. The second reason is that the used solar reflective metamaterial has a solar absorption of approximately 10%, which will collect the solar power and transfer it into heat. The third reason is that content of the atmospheric water vapor in Hefei in May is relatively high, so the sky transmittance within the atmospheric window is damaged. However, although the temperature of the SH/RC device under the *Water case* in this experimental demonstration can not achieve a sub-ambient cooling phenomenon, the proposed strategy can still regulate the temperature within the two cases, which is a positive feature for the tunable thermal management for various applications, such as outdoor cars and building surfaces.

The temperature rise rate of the SH/RC device under the *CNTs case* and the *Water case* is calculated and plotted in Fig. 6. During calculation, the time step is set as 1.0 h. It is found that the temperature rise rate at night is nearly the same and this is because the RC process dominates the heat transfer of two devices. Besides, the device reaches a thermally steady-state during RC mode due to the stable environment condition and absence of solar irradiance, which makes the temperature rise rate of the device at a low level and close to 0°C/h. When the sun rises, the temperature rise rate of the SH/RC device under the *CNTs case* firstly increases rapidly and then decreases. Before noon, the temperature rise rate of the SH/RC device under the *CNTs case* is obviously higher than that under the *Water case*, indicating the good solar thermal ability of the device under the *CNTs case*. In the afternoon, the tendency reverses and this is because the solar irradiance decreases, and the effect of heat dissipation rate is gradually highlighted. Besides, the temperature of the SH/RC device under the *CNTs case* is always higher than that under the *Water case* in the afternoon, and the heat dissipation rate is closely related to the absolute temperature of the device. The higher the SH/RC device's temperature is, the larger the heat dissipation rate of the device occurs.

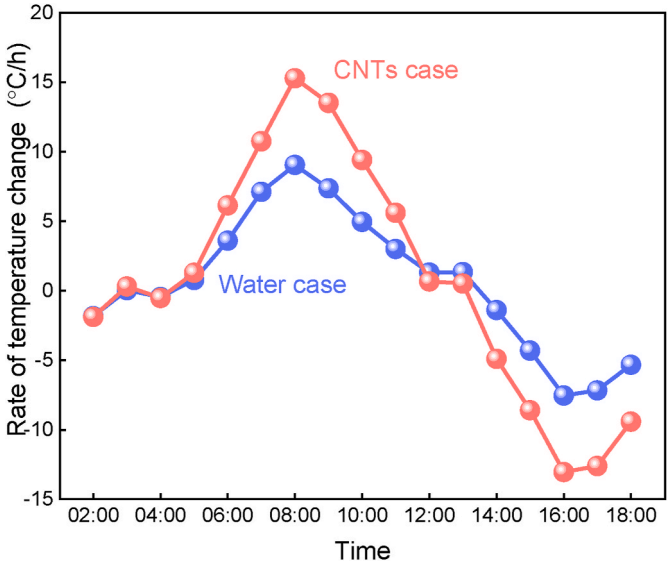

Fig. 6. The temperature rise rate of the SH/RC device under the *CNTs case* and the *Water case* during the testing period.

3. Thermal modeling

3.1. Thermal analysis model

To further explore the tunable thermal management of the proposed strategy, a simulation study is conducted to investigate the thermal performance of the device under different modes. Fig. 7a shows the heat transfer process of the SH/RC device, which relates to the thermal emissive power Q_{rad}, absorbed solar irradiance Q_{sun}, absorbed atmospheric radiation Q_{atm}, and heat loss power caused by convection and conduction process $Q_{non\text{-}rad}$.

According to the first law of thermodynamics, the energy balance of the SH/RC device can be governed by:

$$cm\frac{\partial T}{\partial t} = -\left(Q_{rad} - Q_{atm} - Q_{sun} - Q_{non-rad}\right) \tag{1}$$

where c is the heat capacity of the SH/RC device, m is the mass of the SH/RC device, T is the temperature of the device, and t is the time. The product of heat capacity and the mass of the device is the integration of the silica cavity (the subscript is $_c$) and the media (the subscript is $_m$) that is filled in the device, which can be expressed by:

$$cm = c_c m_c + c_m m_m \tag{2}$$

In Equation (1), the thermal emissive power of the device is given by:

$$Q_{rad} = A\cdot 2\pi \int_0^{\frac{\pi}{2}} \int_0^{\infty} I_{BB}(\lambda,\ T)\varepsilon(\lambda,\ \theta)\ \ sin\theta\ \ cos\theta\ \ d\lambda d\theta \tag{3}$$

where A is the sky-faced area of the SH/RC device, I_{BB} (λ, T) is the spectral radiance of the blackbody at wavelength λ and temperature T, ε (λ, θ) is the spectral-angular emissivity of the device.

Similarly, the absorbed atmospheric radiation can be expressed by:

$$Q_{atm} = A\cdot 2\pi \int_0^{\frac{\pi}{2}} \int_0^{\infty} I_{BB}(\lambda,\ T_a)\varepsilon(\lambda,\ \theta)\ \ \varepsilon_{atm}(\lambda,\ \theta)\ \ sin\theta\ \ cos\theta\ \ d\lambda d\theta \tag{4}$$

where T_a denotes ambient air temperature, ε_{atm} (λ, θ) is the spectral-angular emissivity of the atmosphere. For simplicity, the grey body assumption is used and Equations (3) and (4) can be approximated as:

$$\begin{cases} Q_{rad} = A\cdot\varepsilon\sigma T^4 \\ Q_{atm} = A\cdot\varepsilon_{atm}\varepsilon\sigma T_a^4 \end{cases} \tag{5}$$

where ε is the average emissivity of the SH/RC device, ε_{atm} is the average emissivity of the atmosphere. A widely used correlation that was derived from previous works is used to define the atmospheric emissivity [41]: $\varepsilon_{atm} = 0.741 + 0.0062T_{dew}$ (night) and $\varepsilon_{atm} = 0.727 + 0.0060T_{dew}$ (day), T_{dew} denotes the dew point temperature that can be obtained using the following relation based on the measured ambient temperature (T_a) and relative humidity (RH) [42]:

$$T_{dew} = \frac{243.12\cdot\left[\ln(RH) + \frac{17.62\cdot T_a}{243.12+T_a}\right]}{17.62 - \left[\ln(RH) + \frac{17.62\cdot T_a}{243.12+T_a}\right]} \tag{6}$$

The absorbed solar irradiance can be described by:

$$Q_{sun} = A\cdot\alpha\cdot G \tag{7}$$

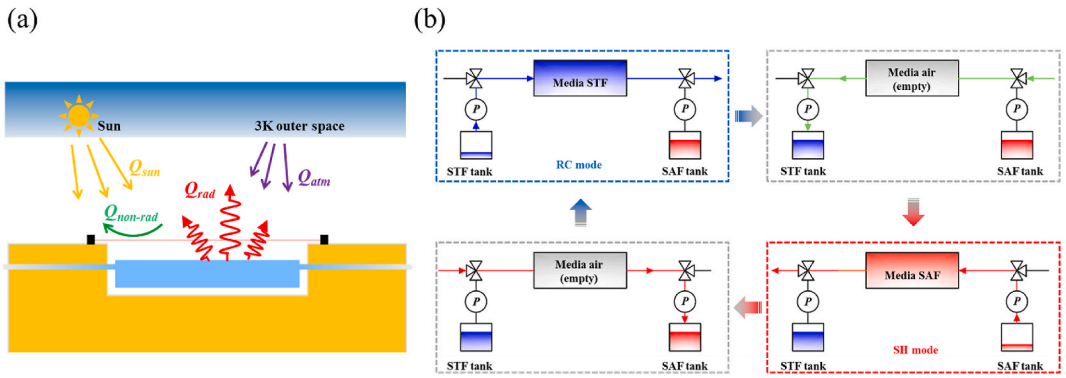

Fig. 7. (a) Schematic showing the heat transfer process of the SH/RC device. (b) Schematic showing a dynamic control of the device between RC mode with solar transparent fluid (STF) filled in the device and SH mode with solar absorption fluid (SAF) media filled in the device.

Where α is the AM 1.5 solar spectrum weighted solar absorptivity of the SH/RC device, G is total solar irradiance.

The non-radiative heat loss power caused by convection and conduction process, $Q_{non\text{-}rad}$, can be modeled by:

$$Q_{non-rad} = A \cdot h \cdot (T - T_a) \tag{8}$$

where h is the overall heat transfer coefficient between the device and ambient air, and the determination of the h is generally related to a correlation that involves the local wind speed (V). In the widely used radiative cooling testing setup, the correlation of h is experimentally determined as $h = 2.5 + 2V$ [33].

By combining the above equations, the transient temperature of the SH/RC device can be calculated once the initial conditions are confirmed. Besides of the heat transfer process simulation of the SH/RC device, a possible switch strategy of RC and SH mode is also proposed and shown in Fig. 7b. Two tanks with solar transparent fluid (STF) and solar absorption fluid (SAF) filled in are integrated into the thermal management system with two tee valves and pumps inserted as auxiliary equipment. In cooling mode, the STF (e.g., deionized water) is pumped from the STF tank and filled into the SH/RC device. When the heating mode is required, the STF in the device is first suction back to the STF tank and the SAF (e.g, CNTs-based fluid) is then pumped into the device for solar absorption, and vice versa.

3.2. Model validation

Before the simulation study, the mathematic model is validated using the experimental data inserted in Fig. 5. The measured meteorological data is input as the boundary conditions. Since the optical properties of the SH/RC device under *CNTs case* is closely related to the optical properties of the CNTs and water, and complex photon transfer processer that includes multiple scattering, direct reflection, and absorption occurs in the SH/RC device under *CNTs case*, the total solar absorptivity of the SH/RC device under *CNTs case* is difficult to accurately obtain. Thus, we choose the SH/RC device under the *Water case* as the validation object. During simulation, the SH/RC device under the *Water case* is simplified as a multilayer structure that consists of a silica layer (1 mm, top layer), a water layer (8 mm, second layer), a silica layer (1 mm, third layer), and a silver layer (200 nm, bottom layer). Besides, the optical constant of the above material is extracted from Refs. [40,43], and the total solar absorptivity of the SH/RC device under the *Water case* is determined using the matric transfer method that is achieved on the MATLAB. As shown in Fig. 8, the simulated temperature of the SH/RC device agrees well with the experimentally measured temperature of the SH/RC device. Besides, the mean relative error (MRE) and the root-mean-square deviation (RMSD) between the simulated and tested temperature values are evaluated to be approximately 9% and 12%, respectively, showing the mathematical model can be accepted for numerical study. It is necessary to note that simulated results are sensitive to the overall heat transfer coefficient between the device and ambient air, and this may be the main reason for the deviation of the simulated results.

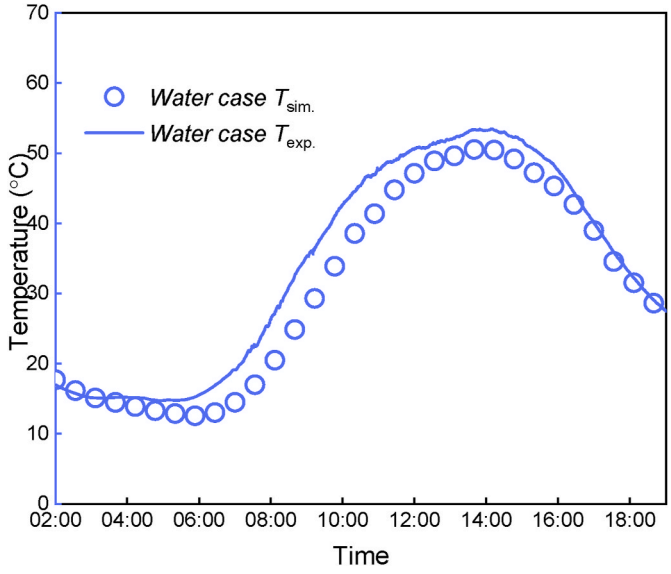

Fig. 8. Simulated and experimental results of the SH/RC device under the *Water case*.

3.3. Tunable temperature management

The main contribution of the proposed strategy is that the temperature of the SH/RC device can be tunably changed using different modes of the device, which can correspondingly adjust the thermal environment of the application. Here, we investigate the tunable temperature control performance of the device under SH and RC modes. During the simulation, a weather condition is required for reference and the measured meteorological data (Fig. 5) is input as the boundary conditions.

First, the solar absorptivity and thermal emissivity of the SH/RC device on the performance of the tunable temperature management are investigated. The solar absorptivity of the SH/RC device is set as 0.9 and 0.1 for SH and RC mode, respectively, and the thermal emissivity of the SH/RC device is set as 0.9. As shown in Fig. 9a, it is clear that the temperature of the device under SH mode is significantly higher than that under RC mode. The maximum temperature difference of the device under SH and RC modes is 60.3°C and the average temperature difference in the noontime (10:00–14:00) is approximately 56.1°C, which

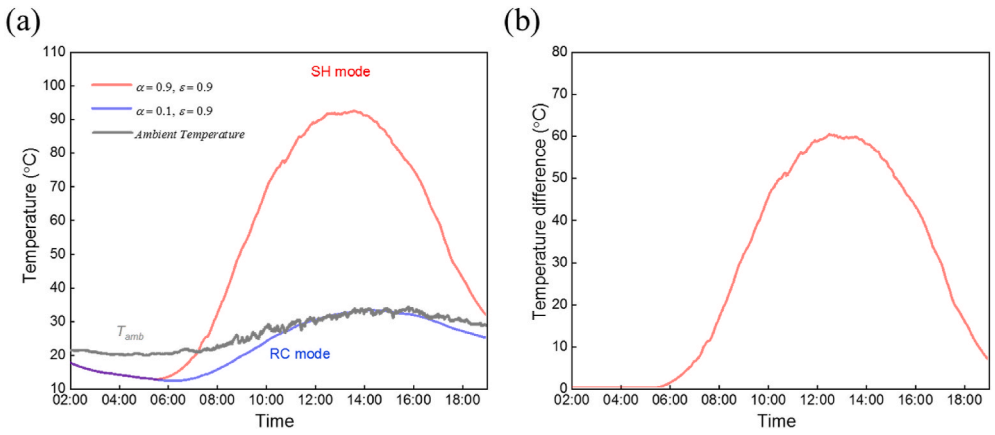

Fig. 9. (a) Temperature of the SH/RC device under SH and RC modes. (b) Temperature difference of the SH/RC device between SH and RC mode.

demonstrates the tunable temperature management ability of the SH/RC device. Notably, the SH/RC device has the potential to achieve sub-ambient radiative cooling during the day if the solar absorptivity of the device is controlled at a low level. Besides, the ST/TC device is only controlled by RC mode at night, so the temperatures of the device under two modes are the same when the solar irradiance is zero.

Second, the effect of the sky condition is investigated since the atmospheric emissivity is also an important factor in addition to the spectral properties of the SH/RC device. During simulation, the relative humidity (RH) of the boundary conditions is respectively changed to be 10%, 50%, and 90%, and the above spectral properties setting (i.e., solar absorptivity of 0.9 and 0.1 for SH and RC, thermal emissivity of 0.9) is also used as input. As shown in Fig. 10a, the temperature difference between the SH/RC device under SH mode and ambient air under RH of 10% is always the lowest at daytime and this is because the atmospheric emissivity under RH of 10% is lower than that under RH of 50% and 90%, which increase the net radiative heat power dissipation and reduce the heat collection ability. For instance, at noon, the temperature difference between the SH/RC device under SH mode and ambient air under RH of 10% is 54.6°C, which is 4.4°C and 6.3°C lower than that under RH of 50% and 90%, respectively. However, the absolute value of temperature difference between the SH/RC device under RC mode and ambient air under RH of 10% is always the highest at daytime and it can also be found that the temperature of the device is always lower than ambient temperature with a maximum and average temperature difference of 17.1°C and 9.6°C, respectively, which means heat dissipation performance of the device under RC mode is enhanced by decreasing RH. Notably, the change of temperature difference plotted in Fig. 10a and b are not proportional to the change of RH, which is because the atmospheric emissivity and RH are non-linear relationships (Fig. 10c).

Third, the temperature of the SH/RC device under different h is also simulated since the convection and conduction heat transfer process also affects the thermal management of the SH/RC device. Fig. 11 shows the temperature of the SH/RC device under different h (1, 5, and 10 W $m^{-2}{\cdot}K^{-1}$) for both SH and RC modes. At night, the sub-ambient cooling phenomenon caused by the RC of the SH/RC device is weakened by the high h since high h corresponds that the device has a strong cooling loss power. At daytime for SH mode, high h means more collected heat of the device is dissipated to the local environment mainly by convection heat between the device and ambient air, which makes the temperature difference between the device and ambient air decrease (Fig. 11a). For example, at noon, the temperature difference between the device and ambient air decreases from 75.3°C to 43.0°C when the h changes from 1 W $m^{-2}{\cdot}K^{-1}$ to 10 W $m^{-2}{\cdot}K^{-1}$. At daytime for RC mode, the high h makes a negative effect on the sub-ambient cooling phenomenon, which is similar to the results obtained at night. Notably, the temperature of the SH/RC device is not sensitive to the h from 13:00 to 17:00 since the temperature of the device is nearly consistent with the ambient temperature and this result can be reflected by the three cures inserted in Fig. 11b.

3.4. Annual temperature management

To further explore the tunable temperature management performance of the proposed strategy and device, an annual simulation study is conducted. During the simulation, the solar absorptivity of the SAF and STF are 0.9 and 0.1, respectively, and the thermal emissivity of the SAF and STF are both 0.9. Besides, the data of the typical meteorological year of Hefei, China is used and the relevant information is presented in Fig. 12. To highlight the tunable temperature control of the device, a control strategy is applied and the detailed process is shown in Fig. 13. The control strategy includes several main principles:

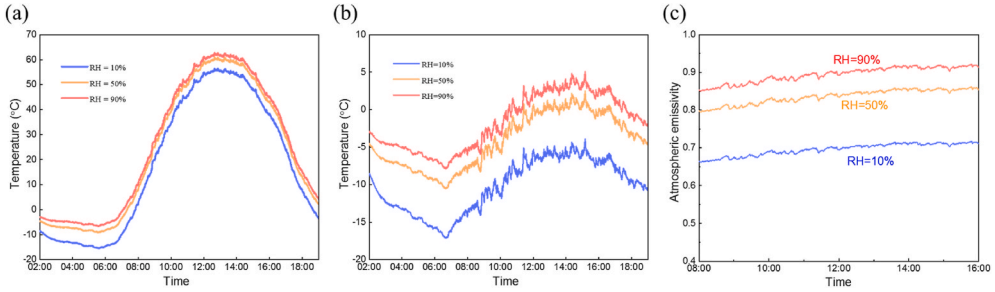

Fig. 10. (a) Temperature difference between the SH/RC device under SH mode and ambient air with RH of 10%, 50%, and 90%, respectively. (b) Temperature difference between the SH/RC device under RC mode and ambient air with RH of 10%, 50%, and 90%, respectively. (b) Calculated atmospheric emissivity with RH of 10%, 50%, and 90%, respectively.

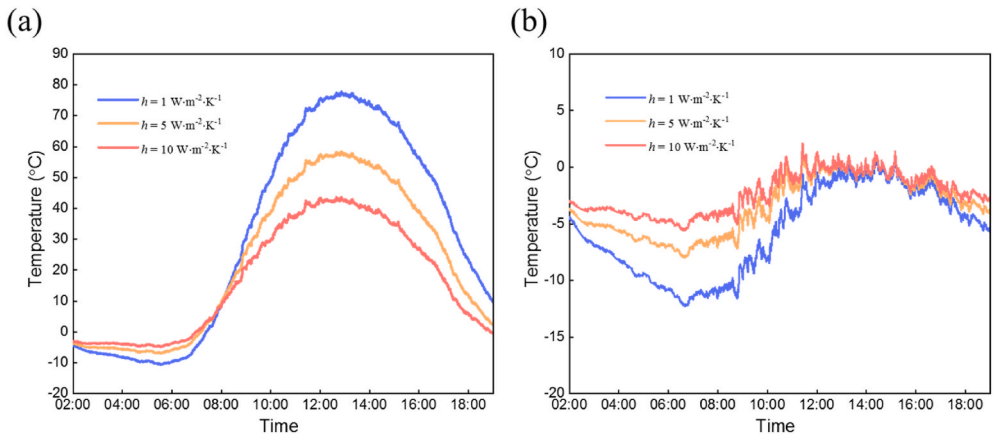

Fig. 11. (a) Temperature difference between the SH/RC device under SH mode and ambient air with h of 1, 5, and 10 W m^{-2}·K^{-1}, respectively. (b) Temperature difference between the SH/RC device under RC mode and ambient air with h of 1, 5, and 10 W m^{-2}·K^{-1}, respectively.

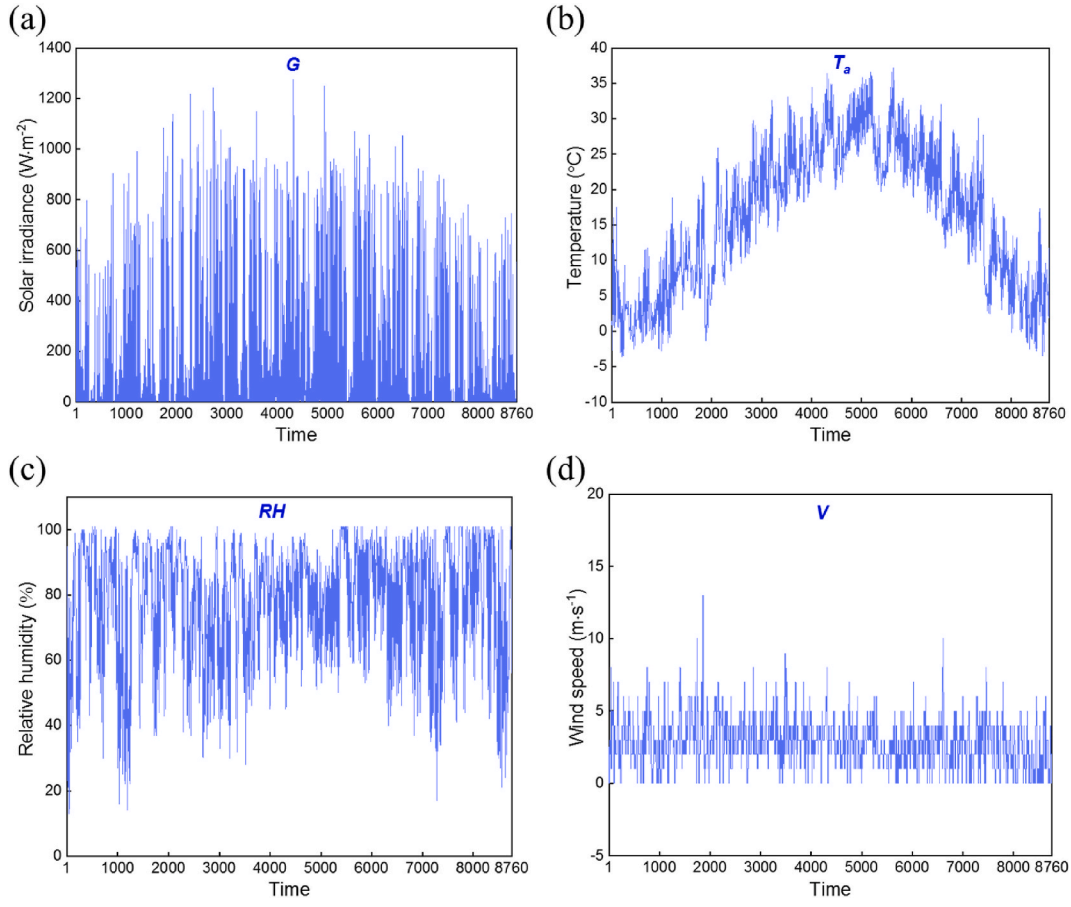

Fig. 12. Typical meteorological data of Hefei, including (a) solar irradiance, (b) ambient temperature, (c) relative humidity, and (d) wind speed.

(i) At daytime, if the device temperature is higher than 26°C, control operations should be made to reduce the device temperature or to make the device temperature at a stable condition.
(ii) At daytime, if the device temperature is lower than 20°C, control operations should be made to increase the device temperature or to make the device temperature at a stable condition.
(iii) At nighttime, the device temperature is independent of SH and RC mode.
(iv) If the media inserted in the device is renewed, the initial temperature of the device is set as the transient ambient temperature.

Here, we provide an example demonstration of the tunable temperature management strategy that is shown in Fig. 13. When the temperature of the device is higher than 26°C, there are several possible conditions for operation adjustments: First, if the ambient temperature is lower than 20°C, the original media inserted in the device should be renewed by the SAF media with ambient temperature. Second, if the ambient temperature is higher than 20°C and the original media inserted in the device is STF, no action is needed. Third, if the ambient temperature is higher than 20°C and the original media inserted in the device is SAF, the media should be renewed by the STF media with ambient temperature. Similar strategies are used for other conditions.

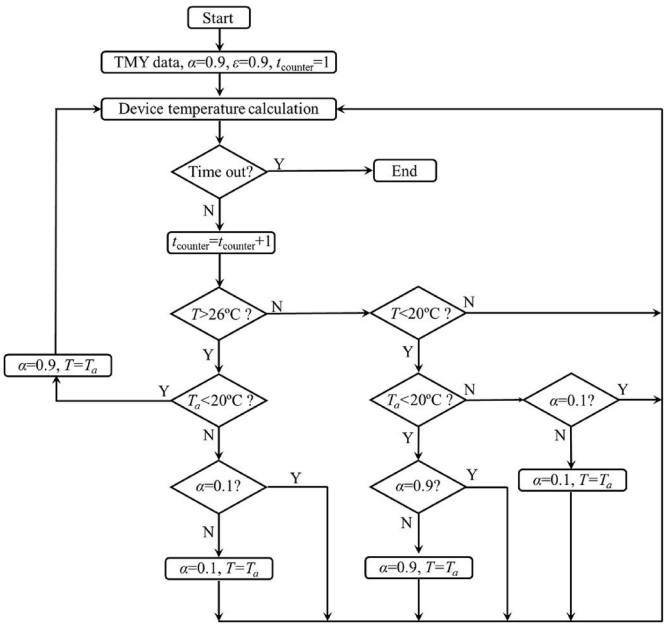

Fig. 13. The flow chart of the tunable temperature management strategy with the SH/RC device.

The calculated temperatures of the device under different modes are calculated and shown in Fig. 14, with ambient temperature given as reference. The temperature of the device under the SH model is higher enough than that under the RC mode at daytime due to the high solar absorption of the SAF (Fig. 14a). Besides, the temperature of the device is nearly 70°C higher than ambient temperature, which will cause an uncomfortable feeling for humans. After using the tunable temperature control strategy, the device temperature at daytime is controlled at a relatively stable state with a maximum temperature of approximately 40°C (Fig. 14b), which is a good feature for active thermal management and can be potentially applied to different backgrounds, including energy-saving buildings. For instance, the accumulated time for the device with dynamical SH and RC modes when its temperature is within 20°C-26°C that is a comfortable temperature region for humans is 2140 h, which is 60.9% and 30.3% higher than that of the device with individual SH and RC mode. Moreover, the device temperature comparison among SH mode, RC mode, and dynamic mode within a small-scale time is also given in Fig. 14c for reference. Notably, the temperature at nighttime cannot be controlled since the thermal emissivity of the current strategy and device is fixed at a high level, but this strategy can be further modified to satisfy the thermal conformant demand at night. Importantly, although the above strategy is proposed based on the temperature threshold values of the device and ambient air, other different strategies can be also developed according to the various requirements. For example, if high temperatures are required for winter and low temperatures are needed for summer, the device can work at SH and RC modes in winter and summer, respectively, and this is a general seasonal operation mode of the device, which is suitable for regions with a typical characteristic of "hot summer and cold winter". Besides, if thermal storage techniques are combined with the proposed strategy, the performance of tunable thermal management can be further improved.

4. Conclusions

In this paper, a strategy that dynamically combines SH and RC

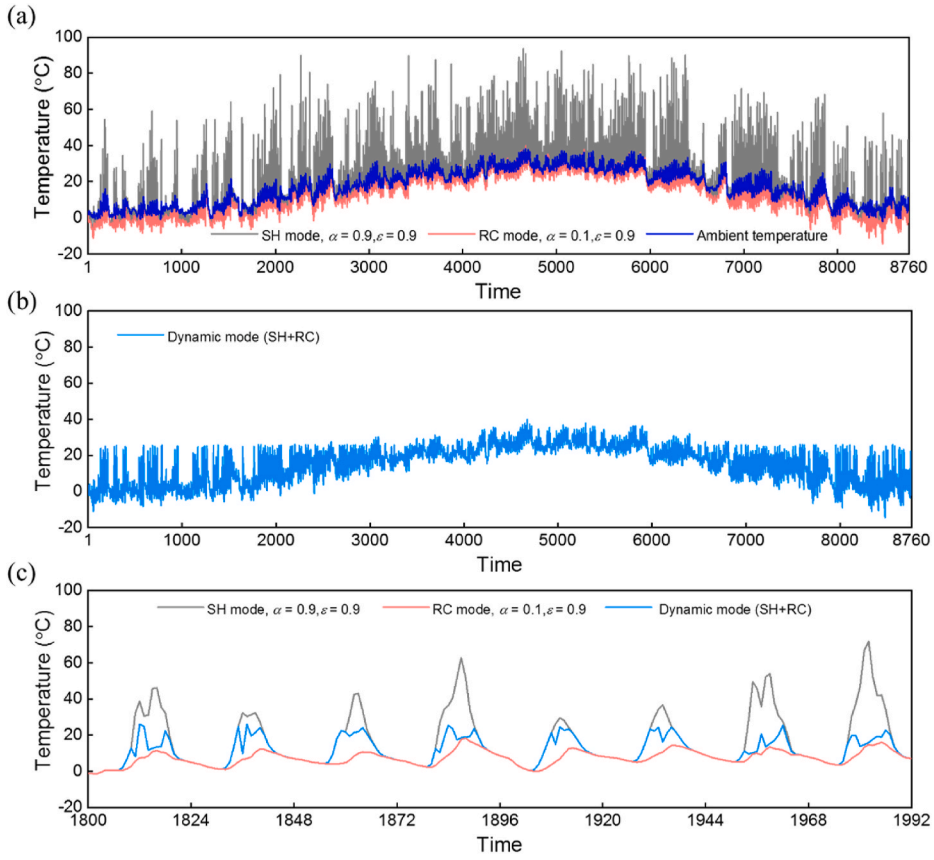

Fig. 14. (a) The annual temperature of the device under SH and RC modes. (b) The annual temperature of the device under tunable modes of SH and RC. (c) The device temperature comparison among SH mode, RC mode, and dynamic mode within a small-scale time.

processes in a single device is proposed for the goal of tunable thermal management. Based on the strategy, the SH/RC device that consists of a transparent silica cavity, SWCNTs aqueous dispersion, solar reflective film, and deionized water is designed and fabricated. An outdoor experiment is conducted to validate the feasibility of the proposed strategy for tunable thermal management. Besides, simulation studies investigate the tunable temperature management ability of the strategy and SH/RC device. The detailed results are summarized as follows:

(1) The SH/RC device with SWCNTs aqueous dispersion filled in (i.e., SH mode) has nearly no solar transmission, corresponding to a high solar absorptivity, which shows that the SH/RC device under SH mode has potential for heat collection. Besides, the SH/RC device with deionized water filled in (i.e., RC mode) can not only achieve strong solar reflection due to the solar transparency of the water and the exists of solar reflective film, but also exhibits high thermal emissivity because of the bulk silica, which indicates the device under RC mode has potential for heat dissipation.
(2) The SH/RC device with SWCNTs media can reach a maximum temperature of 78.9°C and the temperature modulation ability of the SH/RC device is tested to be 26.3°C. Importantly, the temperature modulation ability of the SH/RC device is predicted to be further improved to be 60.3°C by improving the solar absorptivity (i.e., 0.9 for SH mode and 0.1 for RC mode) regulation ability of the device and improving its thermal emissivity (i.e., 0.9).
(3) If the comfortable temperature region for humans is set within 20°C-26°C, the annually cumulative time for the SH/RC device within this region is 60.9% and 30.3% higher than that of the device with individual SH and RC mode, which can save energy consumed for the comfortable artificial environment and this feature can be extended to various applications, such as solving the overheating problem of the commercial solar collectors within the hot seasons.

Data availability

The data that support the findings of this study are available from the corresponding author upon reasonable request.

Declaration of competing interest

The authors declare that they have no known competing financial interests or personal relationships that could have appeared to influence the work reported in this paper.

Acknowledgments

This work was supported by the National Natural Science Foundation of China (NSFC 52106276 and 52130601), Project funded by China Postdoctoral Science Foundation (2020TQ0307 and 2020M682033), and Fundamental Research Funds for the Central Universities (WK2090000028).

References

[1] X. Li, B. Sun, C. Sui, A. Nandi, H. Fang, Y. Peng, G. Tan, P. Hsu, Integration of daytime radiative cooling and solar heating for year-round energy saving in buildings, Nat. Commun. 11 (2020) 6101, https://doi.org/10.1038/s41467-020-19790-x.
[2] Y. Li, C. Lin, Z. Wu, Z. Chen, C. Chi, F. Cao, D. Mei, H. Yan, C.Y. Tso, C.Y.H. Chao, B. Huang, Solution-processed all-ceramic plasmonic metamaterials for efficient solar–thermal conversion over 100–727 °C, Adv. Mater. 33 (2021) 14–17, https://doi.org/10.1002/adma.202005074.
[3] F. Rubbi, L. Das, K. Habib, N. Aslfattahi, R. Saidur, M.T. Rahman, State-of-the-art review on water-based nanofluids for low temperature solar thermal collector application, Sol. Energy Mater. Sol. Cells 230 (2021), 111220, https://doi.org/10.1016/j.solmat.2021.111220.
[4] L. Zhou, X. Li, G.W. Ni, S. Zhu, J. Zhu, The revival of thermal utilization from the Sun: interfacial solar vapor generation, Natl. Sci. Rev. 6 (2019) 562–578, https://doi.org/10.1093/nsr/nwz030.
[5] D. Tschopp, Z. Tian, M. Berberich, J. Fan, B. Perers, S. Furbo, Large-scale solar thermal systems in leading countries: a review and comparative study of Denmark, China, Germany and Austria, Appl. Energy 270 (2020), 114997, https://doi.org/10.1016/j.apenergy.2020.114997.
[6] E. Vengadesan, R. Senthil, A review on recent development of thermal performance enhancement methods of flat plate solar water heater, Sol. Energy 206 (2020) 935–961, https://doi.org/10.1016/j.solener.2020.06.059.
[7] B. Zhao, M. Hu, X. Ao, N. Chen, G. Pei, Radiative cooling: a review of fundamentals, materials, applications, and prospects, Appl. Energy 236 (2019) 489–513, https://doi.org/10.1016/j.apenergy.2018.12.018.
[8] D. Zhao, A. Aili, Y. Zhai, S. Xu, G. Tan, X. Yin, R. Yang, Radiative sky cooling: Fundamental principles, materials, and applications, Appl. Phys. Rev. 6 (2019), 021306, https://doi.org/10.1063/1.5087281.
[9] X. Lu, P. Xu, H. Wang, T. Yang, J. Hou, Cooling potential and applications prospects of passive radiative cooling in buildings: the current state-of-the-art, Renew. Sustain. Energy Rev. 65 (2016) 1079–1097, https://doi.org/10.1016/j.rser.2016.07.058.
[10] M. Zeyghami, D.Y. Goswami, E. Stefanakos, A review of clear sky radiative cooling developments and applications in renewable power systems and passive building cooling, Sol. Energy Mater. Sol. Cells 178 (2018) 115–128, https://doi.org/10.1016/j.solmat.2018.01.015.
[11] R. Yang, X. Yin, Passive cooling in an urban setting, Nat. Sustain. 2 (2019) 663–664, https://doi.org/10.1038/s41893-019-0358-3.
[12] H.H. Al-Kayiem, A.A. Ismaeel, A.T. Baheta, M.A. Aurybi, Performance enhancement of solar vortex power generator by Al2O3-in-black paint coating, J. Clean. Prod. 316 (2021), 128303, https://doi.org/10.1016/j.jclepro.2021.128303.
[13] F. Cao, D. Kraemer, L. Tang, Y. Li, A.P. Litvinchuk, J. Bao, G. Chen, Z. Ren, A high-performance spectrally-selective solar absorber based on a yttria-stabilized zirconia cermet with high-temperature stability, Energy Environ. Sci. 8 (2015) 3040–3048, https://doi.org/10.1039/C5EE02066B.
[14] D. Yang, X. Zhao, Y. Liu, J. Li, H. Liu, X. Hu, Z. Li, J. Zhang, J. Guo, Y. Chen, B. Yang, Enhanced thermal stability of solar selective absorber based on nano-multilayered AlCrSiO films, Sol. Energy Mater. Sol. Cells 207 (2020), 110331, https://doi.org/10.1016/j.solmat.2019.110331.
[15] S. Mesgari, N. Hjerrild, H. Arandiyan, R.A. Taylor, Carbon nanotube heat transfer fluids for solar radiant heating of buildings, Energy Build. 175 (2018) 11–16, https://doi.org/10.1016/j.enbuild.2018.07.002.
[16] D. Wang, Y. Fang, W. Yu, L. Wang, H. Xie, Y. Yue, Significant solar energy absorption of MXene Ti3C2Tx nanofluids via localized surface plasmon resonance, Sol. Energy Mater. Sol. Cells 220 (2021), 110850, https://doi.org/10.1016/j.solmat.2020.110850.
[17] D. Zhao, J. Ji, H. Yu, X. Zhao, A study on thermal characteristic and sleeping comfort of a hybrid solar heating system applied in cold rural areas, Energy Build. 182 (2019) 242–250, https://doi.org/10.1016/j.enbuild.2018.10.027.
[18] H. Yang, Q. Wang, Y. Huang, G. Gao, J. Feng, J. Li, G. Pei, Novel parabolic trough power system integrating direct steam generation and molten salt systems: preliminary thermodynamic study, Energy Convers. Manag. 195 (2019) 909–926, https://doi.org/10.1016/j.enconman.2019.05.072.
[19] P. Tao, G. Ni, C. Song, W. Shang, J. Wu, J. Zhu, G. Chen, T. Deng, Solar-driven interfacial evaporation, Nat. Energy. 3 (2018) 1031–1041, https://doi.org/10.1038/s41560-018-0260-7.
[20] A.P. Raman, M.A. Anoma, L. Zhu, E. Rephaeli, S. Fan, Passive radiative cooling below ambient air temperature under direct sunlight, Nature 515 (2014) 540–544, https://doi.org/10.1038/nature13883.
[21] H. Ma, K. Yao, S. Dou, M. Xiao, M. Dai, L. Wang, H. Zhao, J. Zhao, Y. Li, Y. Zhan, Multilayered SiO2/Si3N4 photonic emitter to achieve high-performance all-day radiative cooling, Sol. Energy Mater. Sol. Cells 212 (2020), 110584, https://doi.org/10.1016/j.solmat.2020.110584.
[22] E. Rephaeli, A. Raman, S. Fan, Ultrabroadband photonic structures to achieve high-performance daytime radiative cooling, Nano Lett. 13 (2013) 1457–1461, https://doi.org/10.1021/nl4004283.
[23] L. Zhu, A.P. Raman, S. Fan, Radiative cooling of solar absorbers using a visibly transparent photonic crystal thermal blackbody, Proc. Natl. Acad. Sci. U.S.A. 112 (2015) 12282–12287, https://doi.org/10.1073/pnas.1509453112.
[24] Y. Zhai, Y. Ma, S.N. David, D. Zhao, R. Lou, G. Tan, R. Yang, X. Yin, Scalable-manufactured randomized glass-polymer hybrid metamaterial for daytime radiative cooling, Science 355 (80-) (2017) 1062–1066, https://doi.org/10.1126/science.aai7899.
[25] J. Mandal, Y. Fu, A.C. Overvig, M. Jia, K. Sun, N.N. Shi, H. Zhou, X. Xiao, N. Yu, Y. Yang, Hierarchically porous polymer coatings for highly efficient passive daytime radiative cooling, Science 362 (80-) (2018) 315–319, https://doi.org/10.1126/science.aat9513.
[26] H. Zhong, Y. Li, P. Zhang, S. Gao, B. Liu, Y. Wang, T. Meng, Y. Zhou, H. Hou, C. Xue, Y. Zhao, Z. Wang, Hierarchically hollow microfibers as a scalable and effective thermal insulating cooler for buildings, ACS Nano (2021), https://doi.org/10.1021/acsnano.1c01814.
[27] Z. Wang, D. Kortge, J. Zhu, Z. Zhou, H. Torsina, C. Lee, P. Bermel, Lightweight, passive radiative cooling to enhance concentrating photovoltaics, Joule 4 (2020) 2702–2717, https://doi.org/10.1016/j.joule.2020.10.004.

[28] B. Zhao, M. Hu, X. Ao, Q. Xuan, G. Pei, Comprehensive photonic approach for diurnal photovoltaic and nocturnal radiative cooling, Sol. Energy Mater. Sol. Cells 178 (2018) 266–272, https://doi.org/10.1016/j.solmat.2018.01.023.
[29] P.-C. Hsu, C. Liu, A.Y. Song, Z. Zhang, Y. Peng, J. Xie, K. Liu, C.-L. Wu, P. B. Catrysse, L. Cai, S. Zhai, A. Majumdar, S. Fan, Y. Cui, A dual-mode textile for human body radiative heating and cooling, Sci. Adv. 3 (2017), e1700895, https://doi.org/10.1126/sciadv.1700895.
[30] M. Zhou, H. Song, X. Xu, A. Shahsafi, Y. Qu, Z. Xia, Z. Ma, M.A. Kats, J. Zhu, B. S. Ooi, Q. Gan, Z. Yu, Vapor condensation with daytime radiative cooling, Proc. Natl. Acad. Sci. U.S.A. 118 (2021), e2019292118, https://doi.org/10.1073/pnas.2019292118.
[31] K. Zhang, D. Zhao, X. Yin, R. Yang, G. Tan, Energy saving and economic analysis of a new hybrid radiative cooling system for single-family houses in the USA, Appl. Energy 224 (2018) 371–381, https://doi.org/10.1016/j.apenergy.2018.04.115.
[32] D.S. Parker, J.R. Sherwin, Evaluation of the NightCool Nocturnal Radiation Cooling Concept : Annual Performance Assessment in Scale Test Buildings, 2008.
[33] D. Zhao, A. Aili, Y. Zhai, J. Lu, D. Kidd, G. Tan, X. Yin, R. Yang, Subambient cooling of water: toward real-world applications of daytime radiative cooling, Joule 3 (2019) 111–123, https://doi.org/10.1016/j.joule.2018.10.006.
[34] J. Liu, Z. Zhou, D. Zhang, S. Jiao, J. Zhang, F. Gao, J. Ling, W. Feng, J. Zuo, Research on the performance of radiative cooling and solar heating coupling module to direct control indoor temperature, Energy Convers. Manag. 205 (2020), 112395, https://doi.org/10.1016/j.enconman.2019.112395.
[35] M. Hu, B. Zhao, X. Ao, Suhendri, J. Cao, Q. Wang, S. Riffat, Y. Su, G. Pei, Performance analysis of a novel bifacial solar photothermic and radiative cooling module, Energy Convers. Manag. 236 (2021), 114057, https://doi.org/10.1016/j.enconman.2021.114057.
[36] L. Zhou, H. Song, N. Zhang, J. Rada, M. Singer, H. Zhang, B.S. Ooi, Z. Yu, Q. Gan, Hybrid concentrated radiative cooling and solar heating in a single system, Cell Reports Phys. Sci. 2 (2021), 100338, https://doi.org/10.1016/j.xcrp.2021.100338.
[37] W. Wang, Z. Zhao, Q. Zou, B. Hong, W. Zhang, G.P. Wang, Self-adaptive radiative cooling and solar heating based on a compound metasurface, J. Mater. Chem. C. 8 (2020) 3192–3199, https://doi.org/10.1039/c9tc05634c.
[38] S. Wang, Y. Zhou, T. Jiang, R. Yang, G. Tan, Y. Long, Thermochromic smart windows with highly regulated radiative cooling and solar transmission, Nano Energy 89 (2021), 106440, https://doi.org/10.1016/j.nanoen.2021.106440.
[39] Z. Fang, L. Ding, L. Li, K. Shuai, B. Cao, Y. Zhong, Z. Meng, Z. Xia, Thermal homeostasis enabled by dynamically regulating the passive radiative cooling and solar heating based on a thermochromic hydrogel, ACS Photonics 8 (2021) 2781–2790, https://doi.org/10.1021/acsphotonics.1c00967.
[40] E.D. Palik, Handbook of Optical Constants of Solids, Academic press, 1985.
[41] P. Berdahl, M. Martin, F. Sakkal, Thermal performance of radiative cooling panels, Int. J. Heat Mass Tran. 26 (1983) 871–880, https://doi.org/10.1016/S0017-9310(83)80111-2.
[42] W. Li, M. Dong, L. Fan, J.J. John, Z. Chen, S. Fan, Nighttime radiative cooling for water harvesting from solar panels, ACS Photonics 8 (2021) 269–275, https://doi.org/10.1021/acsphotonics.0c01471.
[43] Refractive Index, 2019. https://refractiveindex.info/.